Non-contact electromagnetic control of torsional vibrations of a rigid cylinder

Atzampou, Panagiota; Meijers, Peter C.; Tsouvalas, Apostolos; Metrikine, Andrei V.

DOI
10.1007/s11071-024-10365-9

Publication date
2024

Document Version
Final published version

Published in
Nonlinear Dynamics

Nonlinear Dyn
https://doi.org/10.1007/s11071-024-10365-9

RESEARCH

Non-contact electromagnetic control of torsional vibrations of a rigid cylinder

Panagiota Atzampou · Peter C. Meijers · Apostolos Tsouvalas · Andrei V. Metrikine

Received: 20 June 2024 / Accepted: 16 September 2024

Abstract The successful deployment of offshore wind turbines hinges on the installation process, particularly the temporary suspension of the turbine components during assembly. External factors or imbalances in control forces can induce vibrations, emphasizing the need for precise control, especially in the torsional mode, to ensure the delicate alignment required for bolted connections. This paper introduces a contactless technique to control the torsional vibrations of a rigid cylinder using electromagnetic interaction between two magnets, incorporating magnetically-imposed damping and active control algorithms. The magnetically-imposed dissipation is achieved by introducing nonlinear damping into the system, i.e. by controlling the orientation of the field exerted by the electromagnetic actuator. Leveraging the nonlinear coupling of the interaction between the magnets and the modification of the stable equilibrium position, the results show a satisfactory active control performance (low residual error and swift response). The key parameters for control efficiency are identified as the separation distance between the magnets, the fluctuation step of the actuator's magnetic field, and the magnetically-induced stiffness relative to the inherent stiffness of the system. Consequently, the proposed method lays a promising foundation for a non-contact control technique, particularly valuable in offshore wind turbine installations.

Keywords Rotational control · Magnetically-imposed damping · Contactless control · Active vibration control · Magnetic stiffness · Offshore wind turbines

P. Atzampou (✉) · A. Tsouvalas · A. V. Metrikine
Department of Engineering Structures, Delft University of Technology, Stevinweg 1, 2628 CN Delft, The Netherlands
e-mail: p.atzampou@tudelft.nl

A. Tsouvalas
e-mail: a.tsouvalas@tudelft.nl

A. V. Metrikine
e-mail: a.metrikine@tudelft.nl

P. C. Meijers · A. Tsouvalas · A. V. Metrikine
Department of Hydraulic Engineering, Delft University of Technology, Stevinweg 1, 2628 CN Delft, The Netherlands
e-mail: p.c.meijers@tudelft.nl

1 Introduction

To contribute to the ongoing energy transition and decarbonization efforts, Europe has set an ambitious target of installing 29 GW of new offshore wind turbines (OWTs) by 2025, as outlined in a recent report by Wind Europe [1]. In alignment with this objective, OWTs are installed in deeper waters with greater capacities and hence larger dimensions to satisfy the ever increasing energy demand [2].

Critical to the successful deployment of larger turbines is the installation process and, more specifically, the temporary suspension of the components of the OWT before their connection to already installed components; such as the connection of an OWT tower to the transition piece (TP) of a monopile foundation [3]. Throughout this stage, external environmental

Published online: 27 September 2024

excitation or asymmetries in control actuation forces, e.g. active tugger line systems, can induce undesirable vibrations of the suspended component. In conjunction with the translational vibration control of a suspended load [4], the torsional rigid body mode (vibration around the longitudinal axis) becomes noteworthy, influencing the overall effectiveness and duration of the installation process. The precise control of this mode is pivotal, especially for connections that necessitate high precision, such as the widely used bolted flange joints. Controlling the torsional vibrations of the tower during installation can ensure the accurate alignment required for a safe and effective assembly of OWT components. In this paper, a contactless rotational control technique is developed, utilizing electromagnetic interaction between two magnets, incorporating magnetically-induced damping and motion manipulation principles.

Magnetically-induced dissipation finds application across diverse industries in the form of magnetic braking, demonstrating its efficacy in controlling the motion of rotating systems. This method encompasses two techniques: electromagnetic induction-based braking and magnetic attraction-based braking. Electromagnetic actuators are employed in active magnetic bearings for controlling the rotation of ferromagnetic objects in rotating machinery [5–9]. In the automobile sector, Puttewar et al. [10] elucidated electromagnetic brakes that utilize attractive forces to pull the armature, effectively arresting the rotatory motion of the system. Ou et al. [11] introduced a novel design of eddy current magnetic brakes, driven by Faraday's law of induction and the Lorentz force formula for descent devices using arrays of permanent magnets. This technique is extended to upright magnetic braking for building elevators [12], railway vehicles [13] and seismic vibration control of civil engineering structures [14,15]. However, in applications like the installation of OWT, where the components requiring control are made of ferromagnetic materials, such as steel, eddy currents are not a viable alternative for efficient rotation braking. Moreover, the use of electromagnetic actuators capable of changing the magnetic field's direction and extracting energy through interaction with a magnetic object has not been thoroughly investigated yet for motion attenuation purposes.

Rotational control has major advancements through the use of magnetic interactions. In biomedical applications, studies have been conducted on the precise control of the motion (translation and rotation) of micromagnets in arbitrary 3D paths using a group of permanent magnets that could rotate with the help of motors modifying the magnetic field [16–18]. Mahoney & Abbott [19] explored the 5-degree-of-freedom manipulation (motion and orientation control) of a magnetic device using a single rotating permanent magnet attached to robotic arm actuator. The aerospace industry has also leveraged rotational magnetic control for satellites, namely for attitude control and stabilization. In this setting, the control is based on the interaction of three orthogonal current-driven magnetic coils with the Earth's magnetic field [20,21]. Despite the multiple degrees of freedom and the high level of controllability exhibited, these applications pertain to systems of smaller scales, ranging from micro [22] to nano-scale [23].

The present study introduces and investigates the efficient contactless rotational control of a cylinder around its shaft. The control relies on the interaction between a permanent magnet attached to the cylinder and an electromagnetic actuator positioned at a fixed distance from the cylinder's surface. Through manipulation of the orientation of the magnetic field of the actuator, fundamental characteristics of the system can be altered, including the natural frequency (through magnetically-imposed stiffness [24,25]) and the equilibrium position. Two distinct control modes are addressed in this work. The first mode deals with the motion attenuation of a rotating cross-section of a cylinder through magnetic interaction, introducing a nonlinear dissipative force to the dynamical system. The second control mode involves active rotational control and the imposition of a desired angle for the cross-section of the cylinder. In this case, the control scheme goes beyond energy extraction, incorporating the enforcement of a new desired stable equilibrium to the system. Particularly relevant for offshore installations, this mode is well-suited for high-precision connection types.

The novelty of the present paper lies in the application of rotation control for OWT components during the installation and assembly. The proposed control strategy leverages the arrangement of one permanent magnet fixed on the object and one electromagnet, whose effective dipole can rotate around its own axis. The study aims to propose the basis (by studying a lab-scale 1/100 prototype) of an efficient contactless control technique for large-scale offshore wind turbine

components, addressing one of the critical vibration modes of the dynamical system separately. The translational mode has been previously addressed in [4].

The paper is organized as follows: Sect. 2 describes the dynamical system and the methodology employed to modify the system's equilibrium position. Section 3 presents the results of two distinct control cases, accompanied by the respective control strategy schemes. The main conclusions drawn from the study are presented in Sect. 4.

2 Methodology

2.1 Dynamical system and governing equations

A typical dynamical system during an offshore operation is presented in Fig. 1a and consists of a semi-submersible vessel, a crane-payload system (a suspended OWT tower) and a desired target position of installation (a monopile). Here, the degree of freedom studied and controlled is the rotation around the longitudinal axis of the tower (ϕ).

In order to create the base case for the proof of concept of the control technique, the aforementioned system is transformed into a simplified but yet equivalent scaled-down system. The equivalent dynamical system is comprised of a ring of mass m, wall thickness τ, and outer radius R that is free to rotate around its shaft. The studied configuration resembles a cross-section of the suspended tower (as observed from above), while the rotational spring element with stiffness k_s represents the stiffness of the attached cables of the crane. The set-up pertains to a single degree-of-freedom (SDOF) system with two unknown states, namely the angle of rotation ϕ and the angular velocity $\dot{\phi}$. A permanent magnet (PM) is attached to the circumference of the ring at $\phi = 0°$ (static equilibrium), which coincides with the equilibrium of the uncontrolled system. The dipole moment $\boldsymbol{m_c}$ describes the orientation and the strength of the PM. While the strength of the dipole moment of the PM (M_c) is constant, the orientation is forced to follow the rotation of the ring ϕ (Fig. 1b). An electromagnetic actuator (EM) is placed along the x-axis at a given distance d from the PM. The dipole moment of the EM is given as $\boldsymbol{m_f}$ and its polarity as M_f. The orientation of the magnetic dipole of the electromagnetic actuator is represented by the angle θ as shown in Fig. 1b. The parameters of the set-up are quantitatively presented in Table 1. The selected values correspond to a full-scale offshore crane-tower system, scaled down to 1/100 to be suitable for laboratory experiments [4].

The equation of motion (EOM) that governs the angular position of the rotating ring derived by means of the Euler-Lagrange method reads:

$$I_z\ddot{\phi} + k_s\phi = T, \tag{1}$$

where I_z is the mass moment of inertia of the ring around its center, and T is the total external torque acting on the system. The undamped natural frequency (f_n) of the dynamical system is equal to

$$f_n = \frac{\omega_n}{2\pi} = \frac{1}{2}\sqrt{\frac{k_s}{I_z}}, \tag{2}$$

while the exact numerical values are given in Table 1.

In the absence of an additional damping mechanism, the external torque T is equal to the torque induced by the magnetic interaction, which is calculated as follows:

$$T = -\frac{\partial W_m}{\partial \phi}. \tag{3}$$

W_m is the contribution of the two interacting magnetic dipoles to the potential energy and is equal to

$$W_m = -\boldsymbol{m_c} \cdot \boldsymbol{B_{fc}}, \tag{4}$$

where $\boldsymbol{B_{fc}}$ is the magnetic field exerted by the EM to the location of the PM on the ring. The external torque can be expressed as

$$T = \hat{\boldsymbol{k}} \cdot (\boldsymbol{T_m} + (\boldsymbol{r_c} \times \boldsymbol{F_m})), \tag{5}$$

where $\hat{\boldsymbol{k}}$ represents the unit vector of the z-axis (perpendicular to the xy-plane), $\boldsymbol{r_c}$ denotes the vector from the center of the cylinder to the location of the EM. The expressions for the force $\boldsymbol{F_m}$ (exerted by one dipole on another, [26]) and the torque $\boldsymbol{T_m}$ (acting around the center of the dipole generated to align it to the field lines, [27]) are given by

$$\boldsymbol{T_m} = \boldsymbol{m_c} \times \boldsymbol{B_{fc}}, \tag{6a}$$

$$\boldsymbol{F_m} = \nabla\left(\boldsymbol{m_c} \cdot \boldsymbol{B_{fc}}\right), \tag{6b}$$

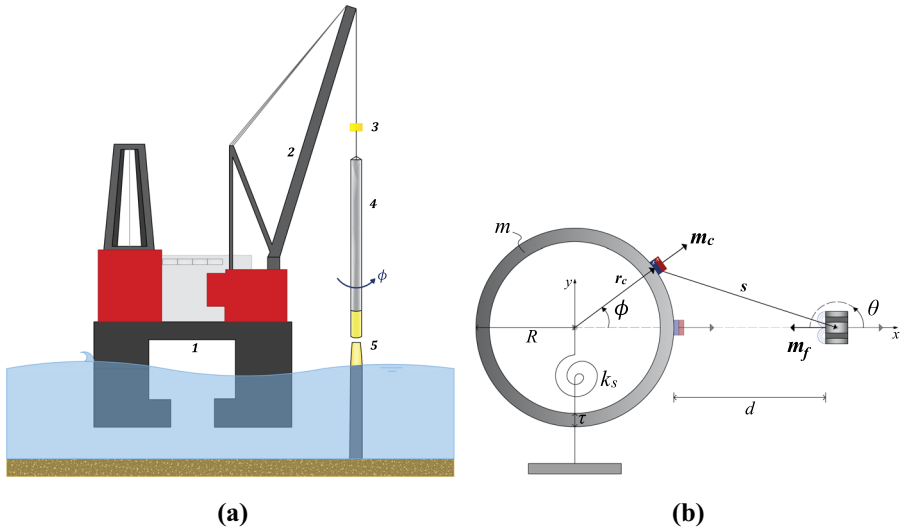

(a) **(b)**

Fig. 1 **a** Annotated diagram of the tower installation: 1. Floating vessel, 2. Heavy lift crane, 3. Lifting block, 4. Wind turbine tower, and 5. Monopile, **b** Schematic diagram of the dynamical system. The ring resembles a cross-section of the tower, while the rotational spring represents the stiffness of the crane cable suspension

Table 1 Set-up parameters of the SDOF system

m (kg)	R (mm)	τ (mm)	k_s (N mm/°)	I_z (kg mm^2)	ω_n (rad/s)	f_n (Hz)
0.2	20.0	2.0	50	36.2	37.2	5.9

with $\boldsymbol{B}_{\boldsymbol{fc}}$ being equal to

$$\boldsymbol{B}_{\boldsymbol{fc}} = -\frac{\mu_0}{4\pi}\nabla\frac{\boldsymbol{m}_{\boldsymbol{f}}\cdot\boldsymbol{s}}{s^3}. \tag{7}$$

The vector representing the separation distance between the two dipoles is denoted as $\boldsymbol{s}$ (Fig. 1b). It is noted that the circumflex $\hat{}$ indicates a unit vector, and a plain character indicates the magnitude of a vector (e.g. $\boldsymbol{s} = s\,\hat{\boldsymbol{s}}$).

Figure 2 illustrates the magnetic field $\boldsymbol{B}_{\boldsymbol{fc}}$ generated by the EM, represented by arrows depicting the field lines and their respective directions. These arrows correspond to normalized values of $\boldsymbol{B}_{\boldsymbol{fc}}$ in space, appearing uniform in size. The contour background of the figure indicates the areas of higher magnetic field strength, with its peak centered at the EM's position. Additionally, white concentric circles and white arrows represent the ring and the orientation of the magnetic dipoles of both the EM and PM respectively. Figure 2a demonstrates the magnetic field generated when the two dipoles are aligned with positive polarities, i.e. the magnets attract each other. An interesting property of the system is observed when the field of the EM is subjected to rotation by a positive angle. In the absence of the linear spring ($k_s = 0$) and presence of linear damping ($T_d = -c_d\dot{\phi}$ with $c_d > 0$), the system rotates and eventually comes to rest at a new static equilibrium position, in this case a negative angle (and vice-versa for a negative rotation of the EM dipole), as depicted in Fig. 2b. The PM dipole adjusts its orientation to align with the external magnetic field lines.

2.2 Potential energy and equilibrium position

To further investigate this property, analysis of the potential energy of the dynamical system is essential. The total potential energy of the system reads

$$W = W_s + W_m, \tag{8}$$

where W_s is attributed to the action of the spring and is equal to

$$W_s = \frac{1}{2}k_s\phi^2. \tag{9}$$

The dynamical system without an external magnet has a static equilibrium dictated solely by the spring element, namely at $\phi = 0°$. Due to the interaction of the two magnets, there is an additional contribution on

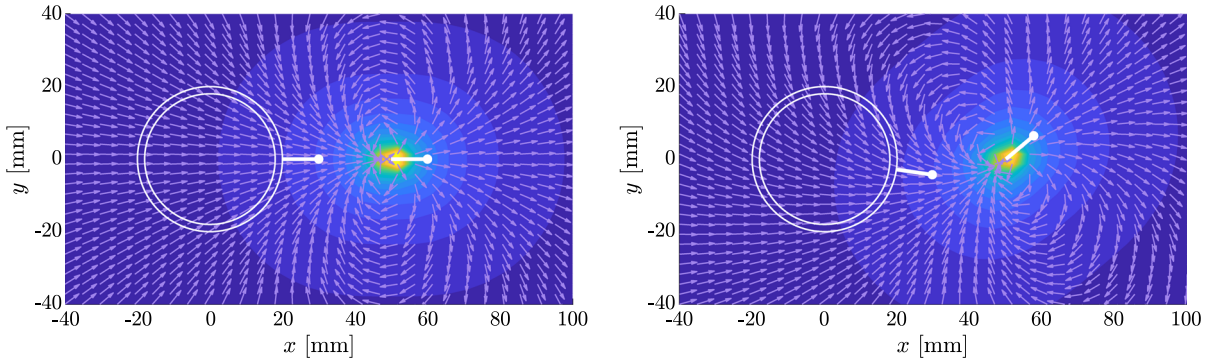

Fig. 2 Spatial distribution of the magnetic field generated by the electromagnetic actuator for different orientations of its field θ

the potential energy W_m (substituting Eqs. (7) to (4)), which reads

$$W_m = -\boldsymbol{m_c} \cdot \boldsymbol{B_{fc}} \tag{10a}$$

$$= \frac{\mu_0 M_c M_f}{4\pi s^3}\left[\cos(\theta-\phi) + \frac{(3R\cos(\theta-\phi) - 3\cos(\theta)(R+d))(\cos(\phi)(R+d) - R)}{s^2}\right], \tag{10b}$$

where s is calculated by

$$s = \sqrt{(R\sin(\phi))^2 + (R + d - R\cos(\phi))^2}, \tag{11}$$

and the magnetic dipoles are given by

$$\boldsymbol{m_f} = M_f \begin{pmatrix}\cos(\theta)\\ \sin(\theta)\end{pmatrix} \text{ and } \boldsymbol{m_c} = M_c \begin{pmatrix}\cos(\phi)\\ \sin(\phi)\end{pmatrix}. \tag{12}$$

Evaluating Eq. (10a) using the Taylor series expansions of the trigonometric terms of ϕ up to the second order around $\phi = 0°$ yields

$$W_m = K_{m_1}\phi^2 + K_{m_2}\phi + C, \tag{13}$$

with:

$$K_{m_1} = \frac{\mu_0 M_c M_f}{4\pi d^5}(6R^2 + 6Rd + d^2)\cos(\theta) \tag{14a}$$

$$K_{m_2} = \frac{\mu_0 M_c M_f}{4\pi d^5}(3Rd + d^2)\sin(\theta) \tag{14b}$$

$$C = -\frac{\mu_0 M_c M_f}{2\pi d^5} d^2 \cos(\theta). \tag{14c}$$

The potential energy W_m (Equations (13) and (14)) illustrates the presence of coupled nonlinear contributions of the rotations of the two dipoles to the potential energy of the system. The magnitude of the magnetically-induced potential energy is proportional to the product of the dipole strengths ($M_f M_c$) and decays as the distance between the two magnets (d) increases.

The equilibrium position of the rotating dynamical system (ϕ_e) is determined by

$$\frac{\partial W}{\partial \phi} = 0 \rightarrow 2K_{m_1}\phi_e + K_{m_2} + k_s\phi_e = 0. \tag{15}$$

Solving for ϕ_e yields

$$\phi_e = -\frac{K_{m_2}}{(2K_{m_1} + k_s)}. \tag{16}$$

It is noted that the equilibrium position is governed by the magnetic interaction when the following condition holds:

$$k_s / K_{m_1} \ll 2. \tag{17}$$

In this case, the closed-form prediction formula for ϕ_e becomes

$$\phi_e = -\frac{1}{2}\left(\frac{3Rd + d^2}{6R^2 + 6Rd + d^2}\right)\tan(\theta_e), \tag{18}$$

where θ_e represents the respective external magnetic field orientation angle to impose the new equilibrium.

Figure 3a plots the nonlinear magnetic potential energy given by Eq. (10a) for different ranges of the angles θ and ϕ, illustrating the potential wells for different angles of rotation of the EM. Equilibrium positions are determined by the local minima of the potential energy. The area with lowest potential energy (stable equilibrium positions) is located in the centre of the plot, confirming that the deepest potential well (and thus most stable equilibrium position) is $\phi_e = 0°$, when the corresponding EM dipole orientation angle $\theta_e = 0°$. This scenario corresponds to perfect alignment of the field lines in attraction. However, when the EM dipole is rotated ($\theta \neq 0°$), the position of the stable equilibrium is shifted, validating the observation made in Fig. 2. The observed rule is that a positive rotation of θ_e results in a negative (but not proportional to θ_e) angle ϕ_e equilibrium position for the system, and vice-versa.

In Fig.3a, the white dotted line connects the lowest points of the potential wells. All these points correspond to the modified equilibrium position ϕ_e for each respective θ_e. Figure 3b displays these lines for different distances d, alongside the formula predicting the equilibrium positions as given by Eq. (18). The latter approximation, as expected, provides a good prediction of the equilibrium positions around $\phi = 0°$, namely for $-6° < \phi_e < 6°$. Therefore, a function can be better fitted to the data that reads

$$\phi_e = A(d)\ \text{arctanh}\,(B(d)\,\theta_e), \tag{19}$$

where for $d = 30\,\text{mm}$ the coefficients of the function are equal to $A = 22.22°$ and $B = -0.0092\,/°$. It is noted that the range of the desired fixed angles in Fig.3b is $-40° < \phi_e < 40°$. This interval corresponds to the range of stable equilibrium angles ϕ_e, namely the adequately deep local minima of the potential (Fig.3a). Therefore, Eq. (19) is chosen to describe the relation between the equilibria and the orientation of the external field in the numerical simulations.

3 Damping control of rotational vibrations

Damping control involves attenuating the vibrations of the system (due to non-trivial initial conditions) to reach the static (intrinsic) equilibrium. The control is based on the introduction of an energy dissipation mechanism into the system using contactless means, namely the magnetic interaction of the PM on the ring and the EM. This control mode is important to initiate the development of the rotation control algorithm envisioned in offshore wind installations. The full-scale counterpart of this mode is the attenuation of the torsional vibrations of a cross-section of a suspended cylindrical structure (resembling an OWT monopile or tower).

3.1 Analysis of the linearized EOM around the intrinsic static equilibrium

To devise a control algorithm for the case where the equilibrium of the system aligns with the desired resting position (control set-point), namely when $\phi_e = 0°$ and $\theta_e = 0°$, it is essential to examine the linearized EOM (valid for small angles ϕ) as derived in Sect. 2.2,

$$I_z\ddot{\phi} + (2K_{m_1} + k_s)\phi + K_{m_2} = 0, \tag{20}$$

with K_{m_1} and K_{m_2} given by Eqs. (14a) and (14b), respectively.

The magnetic interaction between the two dipoles contributes to the stiffness of the system through an additional term K_{m_1}. The coefficient K_{m_1} (for $|\theta|<90°$) is positive when the product of dipole strengths $M_c M_f$ is positive. Additionally, K_{m_2} is a term independent of ϕ, and its sign is determined by either the orientation θ or the polarity M_f of the electromagnetic dipole when $M_c > 0$.

3.2 Control strategy

Motion attenuation within the system can be achieved through a damping mechanism. Coulomb friction is a non-linear dissipative force characterized by the following form [28]:

$$D = \mu_s \text{sign}(v), \tag{21}$$

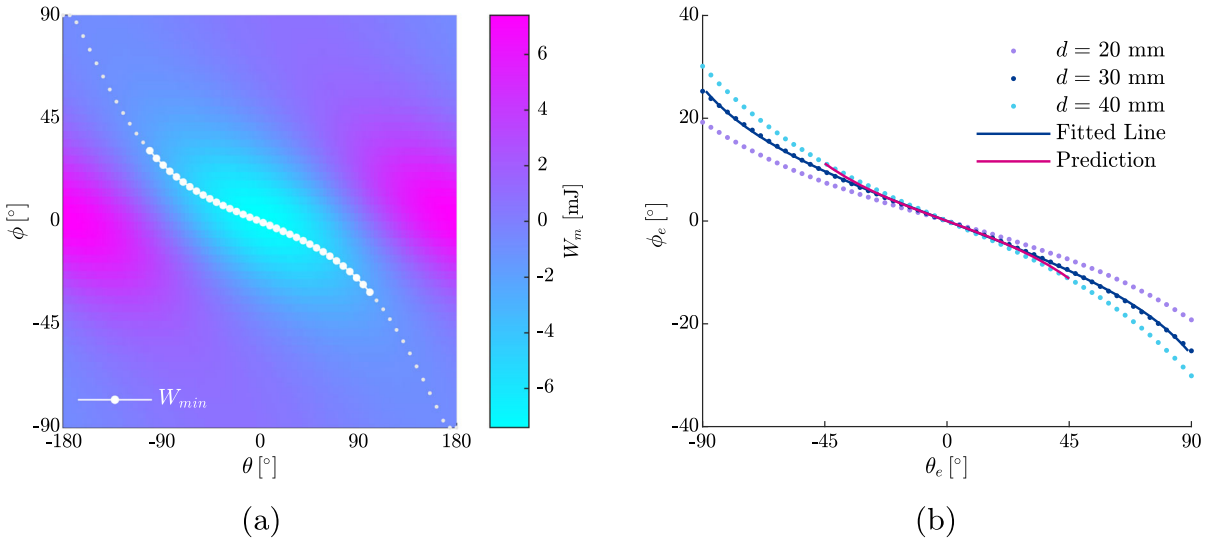

Fig. 3 **a** Potential energy of the dipole W_m for different angles θ and ϕ for $d = 30$ mm, **b** Fitting functions for the prediction of the new equilibrium point ϕ_e and corresponding external magnetic field orientation θ_e for different d

where μ_s represents the kinetic friction coefficient and v denotes the velocity. This force acts as a constant force with a sign opposing the velocity of the system. By examining Eq. (14b), a force resembling Coulomb friction can be introduced into the system either by alternating the polarity M_f or by modifying the orientation of the external field θ.

Selecting the polarity of the actuator as the control variable of the system leads to the adoption of the following expression: $M_f = M_{f_0}\,\text{sign}(\dot{\phi})$, where M_{f_0} corresponds to the constant absolute value of the strength of the EM. Additionally, the orientation angle θ is chosen to be equal to $\theta = \theta_0$, where θ_0 can be any arbitrary, but small, non-zero angle. While this orientation ensures that the damping term K_{m_2} is not eliminated (see Eq. (14b)), it conflicts with the optimal orientation for the intrinsic equilibrium, according to which the two dipoles are aligned to impose $\phi_e = 0°$. It is noted that M_f also dictates the sign of the additional magnetically-induced stiffness K_{m_1}. To avoid the occurrence of negative stiffness, which can lead to instability, the stiffness coefficients must satisfy the following condition:

$$\max(|K_{m_1}|) < \frac{k_s}{2} \rightarrow M_{f_0} M_c < \frac{2\pi d^5 k_s}{\mu_0 (6R^2 + 6Rd + d^2)}, \tag{22}$$

in which, for the given system parameters, $M_{f_0} M_c < 0.88$ is required. Selecting any electromagnetic strength within this specified range results in a stiffness ratio of $k_s / K_{m_1} > 2$, opposing the condition in Eq. (17) for a magnetically-governed response, leading in an overall impractical control solution.

Thus, in order to avoid instability and ensure practical controllability, the control variable is the orientation of the field generated by the EM, which is chosen to fluctuate around $\theta_e = 0°$ with a certain predefined small step $\pm\Delta\theta$. The sign of $\Delta\theta$ is determined by the direction of the angular velocity $\dot{\phi}$, resulting in θ following the rule

$$\theta = \Delta\theta \ \text{sign}\,(\dot{\phi}). \tag{23}$$

For each time step, the controller selects from a number of predefined cases depending on the error from the desired angular position ($e = \phi_e - \phi$). The control cases are:

- Case 0: No action taken (M_f, $\theta = 0°$), when the damping control is successful and the attenuated response is within negligible amplitude bounds ($e < 0.5°$ and $\dot{e} < 50°/s$), and
- Case 1: Positive EM rotation (M_f, $\theta = +\Delta\theta$), or
- Case 2: Negative EM rotation (M_f, $\theta = -\Delta\theta$).

Figure 4 illustrates the damping control strategy scheme adopted based on the aforementioned cases and

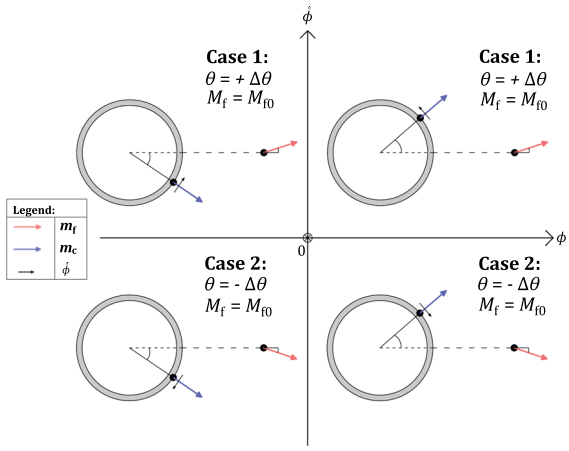

Fig. 4 Phase portrait of the damping control scheme detailing the control cases per quadrant

the phase-space quadrants, ensuring energy extraction. The small fluctuation of the EM dipole orientation aims to generate a torque that opposes the motion of the system, by introducing a force resembling Coulomb friction.

In the examined control scenario, the system initiates from non-trivial initial conditions $(\phi_0, \dot{\phi}_0)$. The desired equilibrium position ϕ_e is set to zero. Euler Forward numerical integration is used to solve the full nonlinear equations of the system, with a time step equal to $\Delta t = 2 \times 10^{-5}$ s, which corresponds to a control frequency $f_s = 50$ kHz. The dynamical system's parameters for the damping control mode are given in Table 2.

3.3 Damping control results

Figure 5a presents the relevant time traces of the controlled motion juxtaposed with the uncontrolled ($\Delta\theta = K_{m_2} = 0$) and linearly damped ($\Delta\theta = 0°$ and $K_{m_2} = c_d\dot{\phi}$ with $c_d = 0.4$ N mm s/°) responses. The controller shows a high level of performance with respect to the attenuation of the rotation angle ϕ and the angular velocity $\dot{\phi}$. The presence of nonlinear damping in the controlled response of the system is apparent from the linear decay of oscillations compared to exponential decay of the linearly damped response. The linear envelope confirms the presence of Coulomb friction in the system [29].

In the time series of the power shown in Fig. 5a, kinetic energy is both extracted and added to the system, which is attributed to the spring-like force introduced to the system by the additional stiffness terms. It is noted that the extraction of energy solely arises from fluctuations in the sign of $\Delta\theta$, which manifest as small-amplitude discontinuities present in the peaks of the torque T. Furthermore, the contribution of magnetic interaction to the stiffness is evident in the change of the natural frequency of the system when comparing the uncontrolled and controlled response. Finally, the magnetic torque required for control is of low amplitude and, as expected, opposes rotation.

The dissipation of motion is explicitly depicted in Fig. 5b, where the phase portrait of the controlled response and the different control cases are illustrated as an inward-spiralling path, contrasting the circular trajectory of the equivalent uncontrolled free vibration. This spiral pattern signifies the presence of damping in the system. Notably, the system states effectively converge to the equilibrium position, $\phi = 0°$ with a small steady-state error of $e \approx 0.4°$. For reference, a linearly damped response with a similar decay rate further illustrates the nonlinear nature of the magnetically-induced damping.

4 Active rotation control

Active rotation control is defined as the imposition of a desired constant angle ϕ_e of the ring, while attenuating the transient response of the system to a set of initial conditions. The desired constant angular position does not coincide with the system's static equilibrium. This mode combines the damping control with active equilibrium manipulation. In real installations, such a controller would be advantageous for component connections that require high precision, such as the bolted flange joints between the tower and the monopile.

Table 2 System parameters for the damping control mode

$M_f M_c$ (A^{2}m^4)	d (mm)	ϕ_e (°)	θ_e (°)	ϕ_0 (°)	$\dot{\phi}_0$ (°/s)	$\Delta\theta$ (°)
5	30	0	0	−10	−100	5

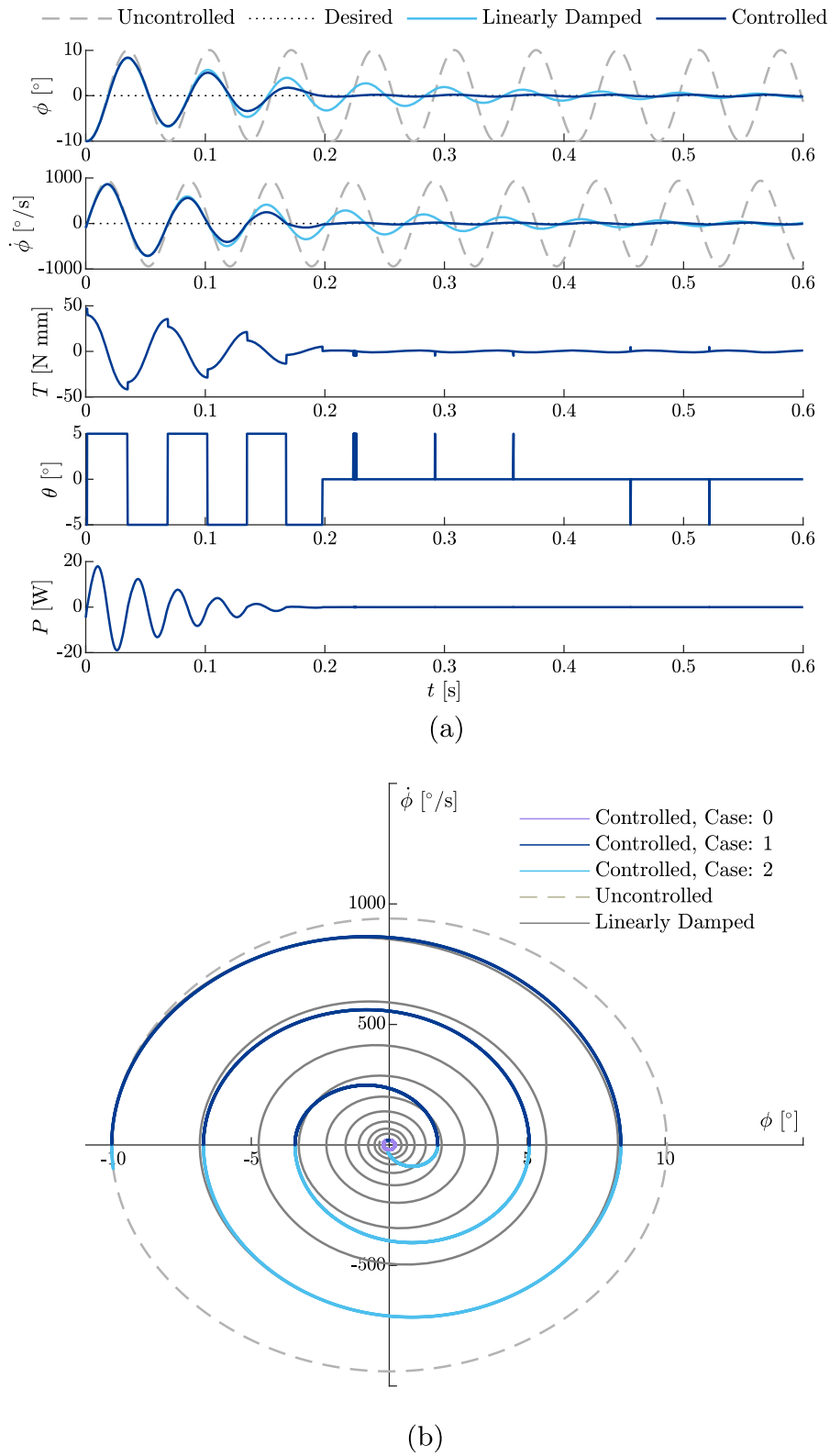

Fig. 5 Damping control system's response: **a** times series of the rotation ϕ and the angular velocity $\dot{\phi}$ of the ring, the actuation torque T, the orientation θ, and the power of the magnetic interaction P, **b** phase portrait of the system's response in the damping control mode

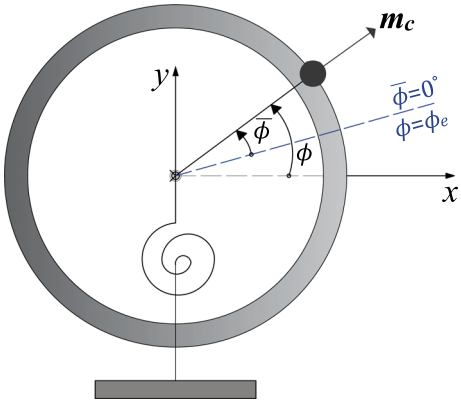

Fig. 6 Definition of the global ϕ and relative $\bar{\phi}$ angle of rotation

4.1 Analysis of the linearized EOM around the desired equilibrium

A similar control strategy to the damping control can also be applied to this control mode, provided that the following transformation is applied:

$$\phi = \bar{\phi} + \phi_e, \tag{24}$$

where $\bar{\phi}$ represents the angular position of the PM relative to the desired equilibrium frame of reference, as depicted in Fig. 6.

Substituting Eq. (24) into the magnetic potential energy W_m Eq. (10a) and expanding the subsequent trigonometric terms of ϕ up to the second order around the relative equilibrium $\bar{\phi} = 0°$, assuming ϕ_e to be a small angle, yields

$$I_z\ddot{\bar{\phi}} + (2K_{m_1} + \Delta K_{m_1} + k_s)\bar{\phi} + (K_{m_2} + \Delta K_{m_2}) = 0, \tag{25}$$

where K_{m_1} and K_{m_2} are given by Eqs. (14a) and (14b) respectively, while

$$\Delta K_{m_1} = -\frac{\mu_0 M_c M_f}{4\pi d^6}\phi_e\,(45R^3 + 63R^2 d + 21Rd^2 + d^3)\,\sin(\theta), \tag{26a}$$

$$\Delta K_{m_2} = +\frac{\mu_0 M_c M_f}{4\pi d^5}\phi_e\,(12R^2 + 12Rd + 2d^2)\,\cos(\theta) = 2K_{m_1}\phi_e. \tag{26b}$$

To impose a new equilibrium that differs from the inherent equilibrium of the system without the magnetic interaction, an additional contribution to the magnetic and spring stiffness is introduced denoted as ΔK_{m_1}. According to Eq. (26a), ΔK_{m_1} acts as a positive contribution to the stiffness, as ϕ_e and the respective θ_e of rotation of the field of the electromagnet have opposite directions. This overall positive additional stiffness prevents the introduction of instability to the dynamical system. Similar to the damping control presented in Sect. 3.2, the dissipative force is introduced to the system through the state-dependent term $K_{m_2} + \Delta K_{m_2}$.

Substituting the equilibrium position ϕ_e (Eq. (16)) as derived by the linearized EOM into Eq. (26b) yields

$$\Delta K_{m_2} = -\frac{2K_{m_1}K_{m_2}}{2K_{m_1} + k_s} \rightarrow K_{m_2} + \Delta K_{m_2} = \frac{k_s}{2K_{m_1} + k_s}. \tag{27}$$

Thus, according to the analysis of the linearized EOM and potential, the state-independent term ΔK_{m_2} is present only when $k_s > 0$.

4.2 Control strategy

Similar to the damping control, the angle of rotation of the electromagnetic field θ serves as the control variable and it follows the rule:

$$\theta = \theta_e + \Delta\theta\ \text{sign}\,(\dot{\phi}). \tag{28}$$

Provided that the desired angle of rotation of the ring does not coincide with the static equilibrium of the system, the methodology outlined in Sect. 2.2 becomes instrumental. Here, for the initial angle of the EM holds: $\theta = \theta_e \neq 0°$. The specific value of θ_e is determined by evaluating Eq. (19) with the prescribed distance d and desired new equilibrium angle ϕ_e. The dynamical system's parameters for the active control mode are given in Table 3.

This control mode consists of two separate actions: the imposition of the new desired equilibrium position and the attenuation of the system's response to the initial conditions. The torque generated by the rotating magnetic field of the actuator consists of a static component due to the constant desired angle θ_e and the additional contribution arising from the modification of this

Table 3 System parameters for active control mode

$M_f M_c$ (A^{2}m^4)	d (mm)	ϕ_e (°)	θ_e (°)	ϕ_0 (°)	$\dot{\phi}_0$ (°/s)	$\Delta\theta$ (°)
50	30	20	−78.3	−10	−100	5

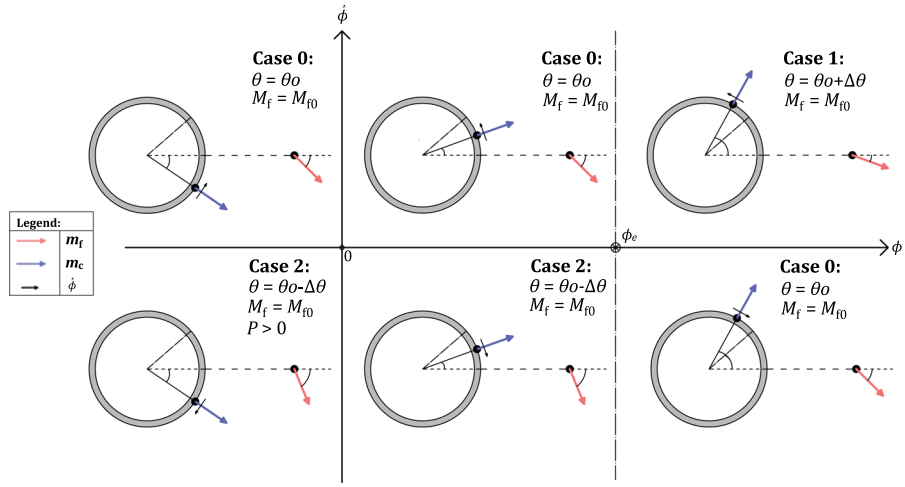

Fig. 7 Phase portrait of the active control scheme detailing the control cases per quadrant

angle $\Delta\theta$. The controller is required to extract ($P < 0$) or add ($P > 0$) energy as necessary to stabilize the system at the chosen new equilibrium position. Therefore, the controller can choose to act according to predefined cases for each time step depending on the error from the desired angular position ($e = \phi_e - \phi = -\bar{\phi}$). include:

- Case 0: No action taken (M_f, $\theta = \theta_e$), when the control was successful and the attenuated response is within certain acceptable amplitude bounds ($e < 1.5°$ and $\dot{e} < 150°/s$), and
- Case 1: Positive EM rotation $\Delta\theta$ (M_f, $\theta_e + \Delta\theta$), or
- Case 2: Negative EM rotation $\Delta\theta$ (M_f, $\theta_e - \Delta\theta$).

Figure 7 illustrates the active control strategy scheme adopted based on the aforementioned cases and the phase-space quadrants, ensuring the condition: $\phi \approx \phi_e$. The controller generates a torque opposite to the system's rotation when the PM deviates from the desired reference angle, with the intention of restoring it to the new equilibrium. The nonlinear EOM is solved through the Euler forward numerical integration with a time step equal to $\Delta t = 2 \times 10^{-5}$ s which corresponds to a control frequency $f_s = 50$ kHz.

4.3 Active rotational control results

The time traces of the controlled motion are presented in Fig. 8a. The controller successfully imposes the new equilibrium with minimal residual error from the desired reference. Moreover, a good level of motion attenuation is achieved, as evidenced by the rotation angle ϕ and angular velocity $\dot{\phi}$ time series, exhibiting the characteristic linear decay indicative of a Coulomb friction dissipative force being present. The efficiency of the nonlinear magnetically-imposed damping becomes evident when compared with the linearly damped response of similar decay rate ($\theta = \theta_e$ and $K_{m_2} = c_d\dot{\phi}$ with $c_d = 0.4$ N mm s/°). The power plot displays energy added and subtracted throughout the simulation, with the slight dominance of negative cycles within the power time signature validating the additional dissipation needed to eliminate the influence of the initial conditions. The nonlinear response of the SDOF system is also observed in the uncontrolled case, particularly in terms of the angular position ϕ, attributed to the interaction of the system with the static component of the EM field. When the electromagnet is activated in static mode (in the uncontrolled case: $M_f = M_{f_0}$, $K_{m_2} = 0$, and $\theta = \theta_e$), it establishes the new equilibrium of the system through

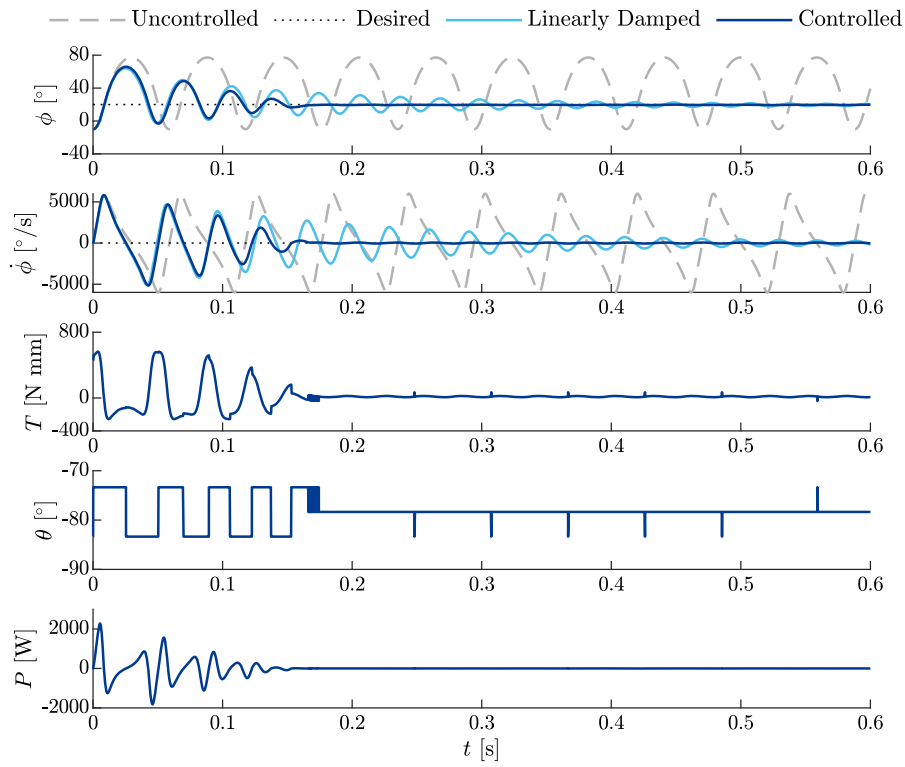

(a)

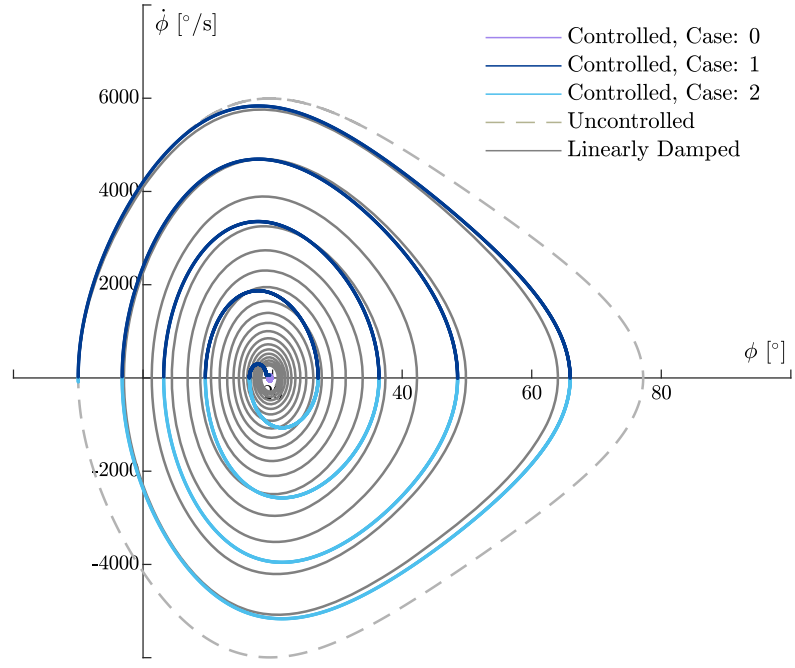

(b)

Fig. 8 Active control system's response: **a** times series of the rotation ϕ and the angular velocity $\dot{\phi}$ of the ring, the actuation torque T, the rotation θ, and the power of the magnetic interaction P, **b** phase portrait of the system's response in the active control mode

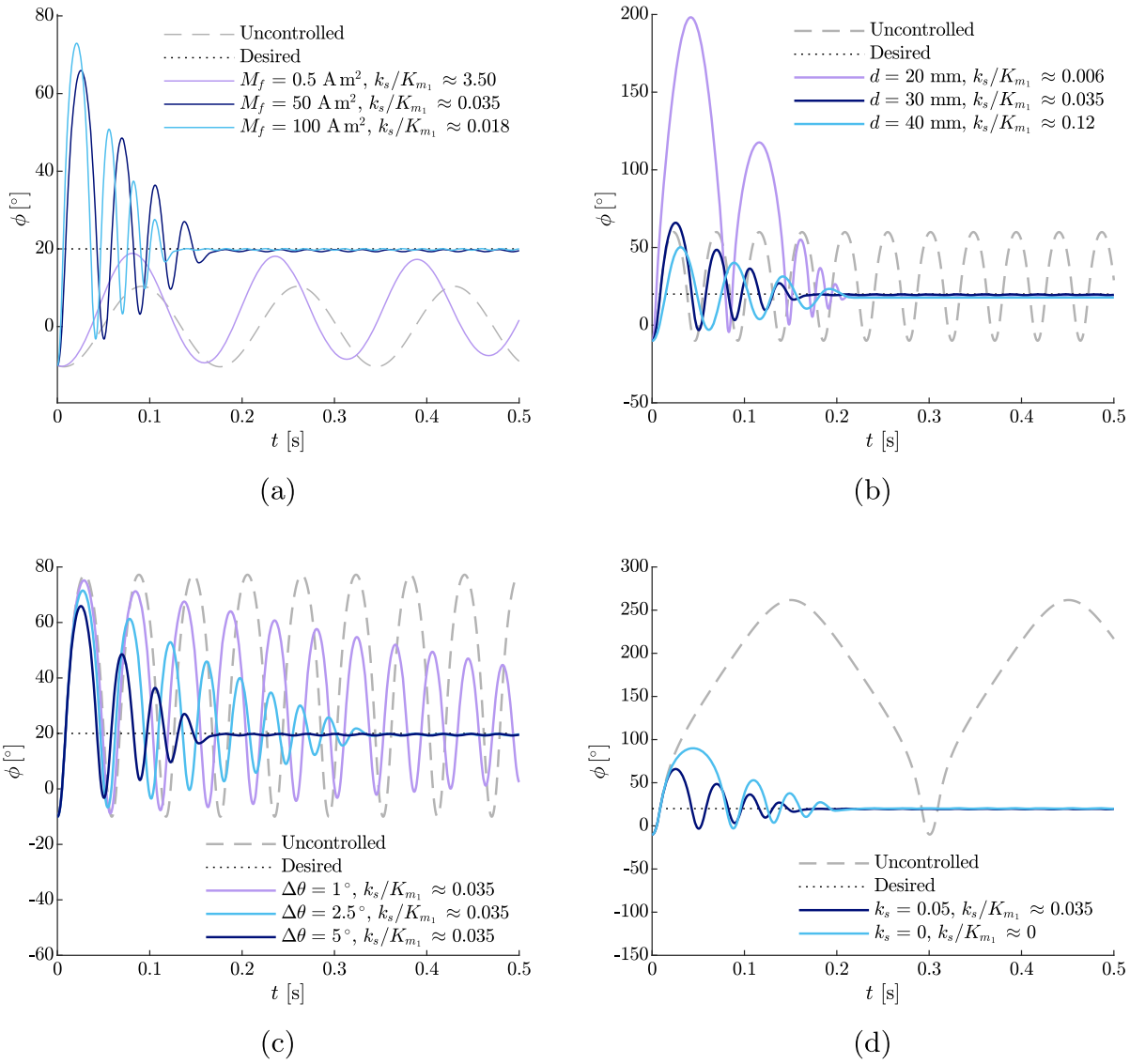

Fig. 9 Comparison of the controlled response of the system for the same initial conditions and varied: **a** magnetic strength M_f with a constant $d = 30$ mm, **b** separation distances d with a constant $M_f = 50$ Am^2, **c** d with a constant $M_f = 50$ Am^2, and **d** spring stiffness k_s with a constant $M_f = 50$ Am^2

a nonlinear adjustment of stiffness, leading to oscillations around ϕ_e.

The phase portrait of the actively controlled response of the system is presented in Fig. 8b. The shape of trajectories is indicative of a dissipative system. It is evident that the damped oscillations of the system converge to the new stable equilibrium with the small error of $e \approx 0.8°$. The nonlinear nature of the static field constantly exerted by the actuator is accountable for the distorted shape of the uncontrolled phase portrait closed loop, which would otherwise be circular in the absence of this magnetic interference.

As anticipated, the control's performance depends highly on the properties of the two magnets and their separation distance. Therefore, an informed choice of $M_f M_c$ and d can improve the controlled response of the system. In Fig. 9a, different magnet strengths M_f (or equivalently different ratios k_s/K_{m_1}) are demonstrated

for the same distance, desired reference and initial conditions. Increasing the strength of the electromagnet reduces the duration of the transient response (the time interval between the initiation of the simulation and the convergence to the desired angle). Moreover, the steady state error e from the desired angle of rotation ϕ_e is reduced by increasing M_f. It is noted that for $k_s/K_{m_1} > 2$ (Eq. (17)), the response is primarily governed by the linear spring, with only a minor shift in the frequency and equilibrium position compared to the uncontrolled response, where only the linear spring is active.

Similar conclusions can be drawn when varying the separation distance d, while the strength and initial conditions are constant (Fig. 9b). Decreasing the separation distance d results in a response with a steeper decay rate. However, due to the non-proportional relation of the distance to the ratio k_s/K_{m_1}, it is imperative to consider upper and lower bounds for the separation distance according to transient behaviour and safety specifications. For instance, a separation distance $d = 20$ mm despite exhibiting the lowest steady state error from the desired resting position, the response is dominated by the high magnetic forces resulting in high rotational angles during the transient response, before the system eventually submitting to the dissipative forces.

Equally important for the control efficiency is the fluctuation step $\Delta\theta$ of the control variable θ. Figure 9c illustrates the controlled responses of the system for various adjustments of the external magnetic field orientation angle, while maintaining the same dipole-to-dipole interaction strength. The effectiveness of the control (demonstrated by a good level of motion attenuation with a short transient) is directly proportional to $\Delta\theta$.

In Fig. 9d, the controlled response of the system is depicted for both the presence ($k_s \neq 0$) and absence ($k_s = 0$) of the linear spring. Despite the restriction that arises from the analysis of the linearized equations (Eq. (27)), the control algorithm effectively imposes the new desired equilibrium. It is important to note that although the control strategy is deduced and designed through the analysis of the linearized analytical equations, the numerical simulations consider the full nonlinear system. The nonlinearity of the system is crucial for the efficiency of the control, allowing it to be effective for higher ϕ_e and independent of the spring when the magnetic interaction is strong enough to impose the new equilibrium.

5 Conclusion

The paper presents a proof of concept for a novel contactless rotation control technique for cylindrical structures rotating around their longitudinal axis, with a specific focus on a potential application in offshore wind turbine installations.

The proposed controller exploits magnetic interaction between two magnets: one permanent magnet fixed on the structure and an electromagnetic actuator, with the control variable being the orientation of the magnetic dipole of the latter. By manipulating the magnetic field in this way, fundamental characteristics of the system, including the natural frequency and the stable equilibrium position, can be modified. Even though, the control strategy is designed by analyzing the linearized controlled system, it demonstrates efficiency in controlling the full nonlinear system solved through the numerical simulations.

High controllability is exhibited in the two control modes studied. The first control mode attenuates the rotational motion of the system by fluctuating the orientation of the external magnetic field, effectively generating a dissipative torque to the system. This energy dissipation is introduced through a magnetically-imposed term resembling Coulomb friction. The second control mode imposes a new stable equilibrium position to the system, combining attenuation with active control of the rotation. A small residual error from the reference and a swift transient response is reported in the active control results. The control performance depends on an informed selection of the separation distance, fluctuation step of the dipole orientation and the ratio between the stiffness of the magnetic interaction and the linear spring.

The findings emphasize the potential for advancing the contactless control technique, especially with the incorporation of additional degrees of freedom and the consideration of intricate dynamics found in offshore applications.

Acknowledgements This contribution belongs to the seventh work plan of the DOT6000-FOX project subsidized by the Rijksdienst voor Ondernemend Nederland (Project ID: TEHE119004) and shared between the partners: Delft University of Technology, Delft Offshore Turbine B.V. (DOT) and Heerema Marine Contractors (HMC).

Author contributions All authors contributed to the conceptualization and design of the manuscript. P.A. (corresponding

author) conducted the simulations, analysis, validation, and visualization, as well as wrote the original draft and prepared the final version of the paper. P.C.M., A.T., and A.V.M. provided guidance and supervision and were responsible for reviewing and editing the draft. Moreover, P.C.M. assisted with the investigation and analysis of the study, while A.T. and A.V.M. were responsible for the funding acquisition and project administration.

Funding The authors have not disclosed any funding.

Data availability No datasets were generated or analysed during the current study.

Declarations

Conflict of interest The authors declare no Conflict of interest.

References

1. Wind Europe: Wind Energy in Europe: 2021 Statistics and the Outlook for 2022–2026. https://windeurope.org/intelligence-platform/product/wind-energy-in-europe-2021-statistics-and-the-outlook-for-2022-2026/
2. Díaz, H., Soares, C.G.: Review of the current status, technology and future trends of offshore wind farms. Ocean Eng. **209**, 107381 (2020)
3. Mehmanparast, A., Lotfian, S., Vipin, S.P.: A review of challenges and opportunities associated with bolted flange connections in the offshore wind industry. Metals **10**(6), 732 (2020)
4. Atzampou, P., Meijers, P.C., Tsouvalas, A., Metrikine, A.V.: Contactless control of suspended loads for offshore installations: proof of concept using magnetic interaction. J. Sound Vib. 118246 (2024)
5. Allaire, P., Kasarda, M., Humphris, R., Lewis, D.: Vibration reduction in a multimass flexible rotor using a midspan magnetic damper. In: Magnetic Bearings: Proceedings of the First International Symposium, 149–158 (1988). Springer
6. Filatov, A., Hawkins, L., McMullen, P.: Homopolar permanent-magnet-biased actuators and their application in rotational active magnetic bearing systems. Actuators **5**, 26 (2016). MDPI
7. Du, T., Geng, H., Wang, B., Lin, H., Yu, L.: Nonlinear oscillation of active magnetic bearing-rotor systems with a time-delayed proportional-derivative controller. Nonlinear Dyn. **109**(4), 2499–2523 (2022)
8. Saeed, N., Kandil, A.: Lateral vibration control and stabilization of the quasiperiodic oscillations for rotor-active magnetic bearings system. Nonlinear Dyn. **98**(2), 1191–1218 (2019)
9. Takam, W.S., Kongne, A.M., Yemélé, D.: Nonlinear dynamics of two dimensional rotor-active magnetic bearing system with generalized-pole legs: stability state diagram and control strategy. Nonlinear Dyn. **111**(19), 17909–17937 (2023)
10. Puttewar, A.S., Kakde, N.U., Fidvi, H.A., Nandeshwar, B.: Enhancement of braking system in automobile using electromagnetic braking. IOSR J. Mech. Civ. Eng. **11**, 54–59 (2014)
11. Ou, F.-M., Wu, Y.-C., Wu, C.-F.: Conceptual design and analysis of a novel magnetic braking descent device. In: IFToMM World Congress on Mechanism and Machine Science, 269–278 (2023). Springer
12. Jou, M., Shiau, J.-K., Sun, C.-C.: Design of a magnetic braking system. J. Magn. Magn. Mater. **304** (2006). https://doi.org/10.1016/j.jmmm.2006.01.149
13. Galardi, E., Meli, E., Nocciolini, D., Pugi, L., Rindi, A.: Development of efficient models of magnetic braking systems of railway vehicles. Int. J. Rail Transport. **3**(2), 97–118 (2015)
14. Zhang, H., Chen, Z., Hua, X., Huang, Z., Niu, H.: Design and dynamic characterization of a large-scale eddy current damper with enhanced performance for vibration control. Mech. Syst. Signal Process. **145**, 106879 (2020)
15. Mazza, F., Labernarda, R.: Magnetic damped links to reduce internal seismic pounding in base-isolated buildings. Bull. Earthq. Eng. **18**(15), 6795–6824 (2020)
16. Sakuma, H.: Three-dimensional motion control of an untethered magnetic object using three rotating permanent magnets. Sci. Rep. **13**(1), 18052 (2023)
17. Shao, Y., Fahmy, A., Li, M., Li, C., Zhao, W., Sienz, J.: Study on magnetic control systems of micro-robots. Front. Neurosci. **15**, 736730 (2021)
18. Ranzoni, A., Janssen, X.J., Ovsyanko, M., IJzendoorn, L.J., Prins, M.W.: Magnetically controlled rotation and torque of uniaxial microactuators for lab-on-a-chip applications. Lab Chip **10**(2), 179–188 (2010)
19. Mahoney, A.W., Abbott, J.J.: 5-dof manipulation of an untethered magnetic device in fluid using a single permanent magnet. Robotics: Sci. Syst. (2014)
20. Silani, E., Lovera, M.: Magnetic spacecraft attitude control: a survey and some new results. Control Eng. Pract. **13**(3), 357–371 (2005)
21. Ovchinnikov, M.Y., Roldugin, D.: A survey on active magnetic attitude control algorithms for small satellites. Prog. Aerosp. Sci. **109**, 100546 (2019)
22. Ryan, P., Diller, E.: Magnetic actuation for full dexterity microrobotic control using rotating permanent magnets. IEEE Trans. Rob. **33**(6), 1398–1409 (2017)
23. Inamori, T., Wang, J., Saisutjarit, P., Nakasuka, S.: Jitter reduction of a reaction wheel by management of angular momentum using magnetic torquers in nano-and micro-satellites. Adv. Space Res. **52**(1), 222–231 (2013)

24. Kanj, A., Thanalakshme, R.P., Li, C., Kulikowski, J., Bahl, G., Tawfick, S.: Design, dynamics, and dissipation of a torsional-magnetic spring mechanism. Mech. Syst. Signal Process. **179**, 109307 (2022)
25. Meijers, P., Atzampou, P., Metrikine, A.: Experimental and numerical study of a magnetic pendulum. In: Third International Nonlinear Dynamics Conference - NODYCON2023 (2023)
26. Yung, K.W., Landecker, P.B., Villani, D.D.: An analytic solution for the force between two magnetic dipoles. Magn. Electr. Sep. **9** (1970)
27. Landecker, P.B., Villani, D.D., Yung, K.W.: An analytic solution for the torque between two magnetic dipoles. Magn. Electr. Sep. **10** (1970)
28. Sulollari, E., Dalen, K., Cabboi, A.: Vibration-induced friction modulation for a general frequency of excitation. J. Sound Vib. **573**, 118200 (2024)
29. Torzo, G., Peranzoni, P.: The real pendulum: theory, simulation, experiment. Lat. Am. J. Phys. Educ. (2009)